Journal of Power Sources 196 (2011) 3420–3425

Contents lists available at ScienceDirect

Journal of Power Sources

journal homepage: www.elsevier.com/locate/jpowsour

Identifying battery aging mechanisms in large format Li ion cells

Matthieu Dubarry[a], Bor Yann Liaw[a,*], Mao-Sung Chen[b], Sain-Syan Chyan[c], Kuo-Chang Han[c], Wun-Tong Sie[c], She-Huang Wu[b]

[a] Hawaii Natural Energy Institute, SOEST, University of Hawaii at Manoa, Honolulu, HI 96822, USA
[b] Department of Materials Engineering, Tatung University, 40 Chungshan N. Rd., Sec. 3, Taipei 104, Taiwan
[c] Chung-Shan Institute of Science and Technology, 481 Jia An Sec., Zhongzheng Rd., Longtan Township, Taoyuan 325, Taiwan

ARTICLE INFO

Article history:
Received 1 April 2010
Received in revised form 2 June 2010
Accepted 10 July 2010
Available online 17 July 2010

Keywords:
Large format
$LiFePO_4$ batteries
Incremental capacity analysis
Thermal degradation
High temperature effect
Loss of lithium inventory

ABSTRACT

Large format $LiFePO_4$-based Li-ion batteries are rapidly becoming available from commercial cell manufacturers. In this paper two types of 10 Ah single cells (one prismatic and another cylindrical) from two manufacturers were tested at room temperature and 60 °C. Both cells suffered severe degradation at 60 °C. The results were analyzed using incremental capacity analysis (ICA) along with other electrochemical techniques. Overall the two types of cells were similar in behavior, despite subtle differences in performance. This study shed some light on the degradation process associated with these two large format $LiFePO_4$ cell designs with regard to thermal degradation at elevated temperatures. The analysis illustrates a unique capability of using ICA to differentiate cell performance and material utilization in different cell designs.

1. Introduction

The pioneer work by Padhi et al. [1] has made olivine-structured $LiFePO_4$ (LFP) battery a competitive energy storage device for smart grid or electric vehicle applications [2–4] along with those based on $LiMn_2O_4$ (spinel), $LiCoO_2$, $LiNiO_2$, or $LiNi_{1/3}Co_{1/3}Mn_{1/3}O_2$ (layer-structured) chemistries [5–8]. Nevertheless, significant capacity degradation has been reported when LFP cells were cycled at elevated temperatures [9,10], suggesting problems with iron dissolution in acidic conditions in $LiPF_6$ electrolytes [9–12] and subsequent deposition of iron on the surface of negative electrode. This iron deposit was believed to act as a catalyst in promoting growth of SEI layer [9]. It was also suggested that some parasitic reaction might occur at high voltages, due to decomposition of electrolyte [13] leading to wetting problems in the electrodes and loss of active material.

The identification of aging and degradation mechanisms in a battery in real-life operation has been a long-desired yet challenging goal in battery R&D and practical applications. Battery aging and degradation often encounter multiple complex and coupled physical–chemical processes in complicated operating conditions, including dynamic duty cycles, temperature/thermal effects, time between operations, and other environmental factors. To quantify aging and degradation effect accurately is not a simple task either. Even if a vigorous test plan can reveal how much capacity is lost in a life cycle test, the result is insufficient to either provide detailed information on degradation mechanism or predict how much loss will occur under a different regime. Only recently incremental capacity analysis (ICA) was demonstrated [14,15] to be explicitly capable of identifying degradation mechanism in combination with high fidelity and accurate computer model simulation. In this work, advancement in applying ICA to decipher aging and degradation mechanisms on large format commercial LFP cells is illustrated.

In previous studies [14,15] in situ, non-invasive electrochemical techniques, including ICA, have been illustrated very powerful in providing detailed information to identify degradation in LFP cells, primarily due to loss of lithium inventory followed by loss of active material [14]. The same techniques can be effective in revealing electrode designs, including grain size and dopant effects [15] in the positive electrode. In this study, origins of capacity loss in degradation in two types of large format (>10 Ah) commercial LFP cells were investigated. The degradation mechanisms at the elevated temperature were discussed.

2. Experimental

Two types of large format (>10 Ah) LFP cells, denoted as "Cell L" and "Cell P", were purchased from two manufacturers, respectively. Table 1 summarizes the specifications for the cells. Cell testing was

* Corresponding author. Tel.: +1 808 956 2339; fax: +1 808 956 2336.
E-mail address: bliaw@hawaii.edu (B.Y. Liaw).

0378-7753/$ – see front matter © 2010 Elsevier B.V. All rights reserved.
doi:10.1016/j.jpowsour.2010.07.029

Table 1
Specifications of the commercial cells used in the study.

Specifications	Cell Label	
	Cell L	Cell P
Shape and geometry	Cuboids (7 cm × 3.5 cm × 8 cm)	Cylinder (H: 13.5 cm, d: 4 cm)
Weight	410 g	380 g
Working potential	3.3 V	3.4 V
Rated capacity	10 Ah	10 Ah
Cell assembly	Flat plates jelly-rolled and interconnected	Cylindrically wound
Vendors	Taiwan	Taiwan

performed by the Energy Storage Materials Laboratory of Tatung University in Taiwan using a multichannel battery tester (GBT-2001i, GW INSTEK). An initial characterization was conducted to assess if all cells from the manufactures were uniform in performance. The regimen used in the initial characterization began with a C/10 charge regime, followed by a 3-h rest, and then a C/10 discharge regime to assess the capacity of the cells. Subsequently, 5 C/2 cycles were executed to condition the cells and determine their rated capacity. The results of the characterization provide the baseline performance of the cells. The resolution of the multichannel tester is 1 mV and 3 mA. Time interval for data recording was 30 s. Temperature-controlled isothermal experiments were performed in an environmental chamber (circulator oven D045, Deng Yang). Cells were allowed for 3-h rest before commencing test regime at the high temperature.

In the life cycle tests, Cell L was first characterized at 25 °C with a procedure comprises 10 cycles of charge–discharge regime at C/10 and 5 cycles with C/10 charge and C/2 discharge. Cell L was then subjected to 1 C/10 cycle and 100 cycles of C/10 charge and C/2 discharge regime at 60 °C. The end-of-charge (EOC) cutoff condition comprises a typical cutoff voltage at 4.2 V and a capacity limit of 10 Ah. At the end of the life cycle test, 10 additional C/10 cycles were carried out at 60 °C.

Cell P was tested using a different test plan and protocol. A C/10 cycle was conducted first, followed by four cycles of C/10 charge and C/2 discharge regime. Such a five-cycle regime was repeated at 25 and 60 °C.

The data and presentations used in the illustration and discussion in this paper are selected from representative cells in each type that are worth discussion or comparison. Therefore, the results generally reflect the behavior of each type of cells.

3. Results

Fig. 1(a) displays the voltage vs. capacity curves in the first few cycles of Cell L at 25 °C. Little change was observed among the first 15 cycles. The cell delivered 11.35 Ah at C/10 and 11.14 Ah at C/2. Fig. 1(b) shows similar curves in the first 5 cycles of Cell P. The cell delivered a higher capacity with 13.38 Ah at C/10 and 13.07 Ah at C/2.

Although the shape of discharge curves appears similar, Cell P released more capacity in the low voltage range than Cell L. In comparison, below 2.75 V; Cell L delivered 2.5% and 3% capacity at C/10 and C/2, while Cell P delivered 4.5% and 6.5%, respectively.

There is a difference in polarization resistance between the two cells at 25 °C. In Cell L voltage variation between C/10 and C/2 was $\Delta V = 80$ mV, whereas in Cell P it was 100 mV. Using Ohm's law approximation (where a linear polarization was observed in the cell), Cell P exhibited a normalized resistance of 250 mΩ Ah, whereas Cell L was at 200 mΩ Ah. Other cells tested under different test regimes also gave results on the same order of magnitude.

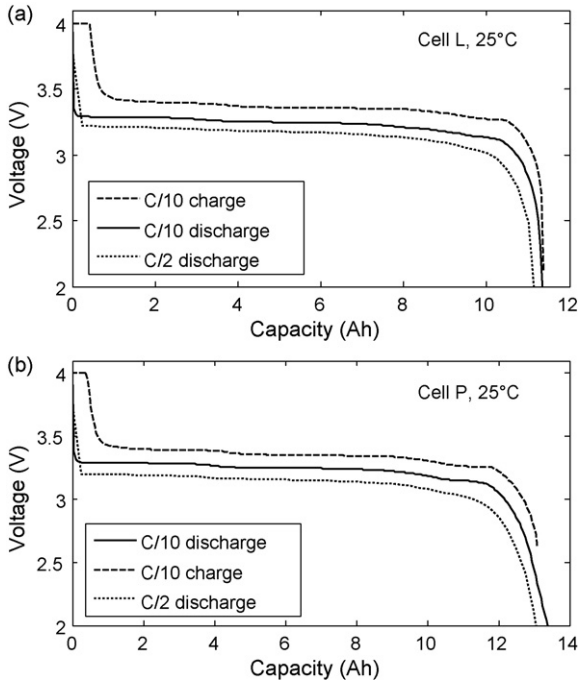

Fig. 1. (a) Voltage–capacity (V vs. Q) curves for Cell L in the first 15 cycles at 25 °C. The cell was charged at C/10 and discharged at C/10 for the first 10 cycles and C/2 for the following 5 cycles. (b) Voltage–capacity curves for Cell P in the first 5 cycles at 25 °C.

Fig. 2 shows the first few discharge regimes in each cell obtained at 60 °C. For both cells, the first discharge regime was at C/10 followed by C/2. Cell L delivered 11.25 Ah (cell was fully charged at C/10 first) at C/10 and 9.9 Ah for the first C/2 discharge, 89% of its capacity at 25 °C. Such low capacity retention at C/2 was due to the capacity cutoff in the charge regime where only 10 Ah were allowed to be recharged. Cell P retained 13.26 Ah (99%) at C/10 and

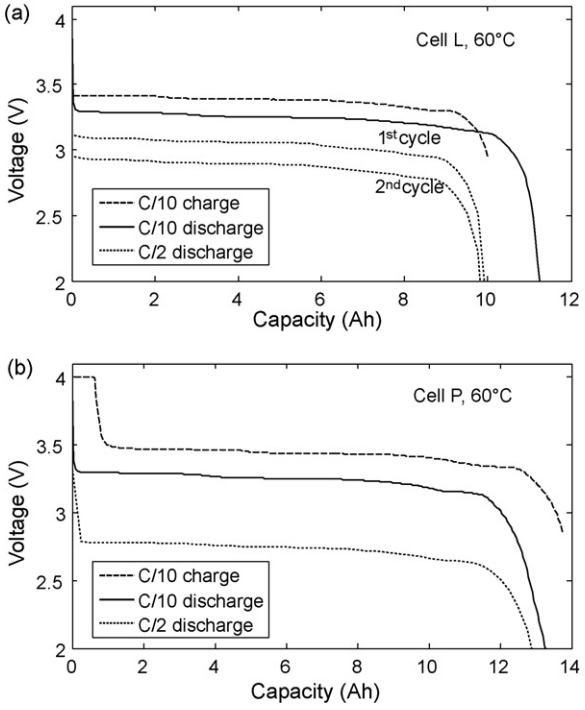

Fig. 2. (a) Cell L voltage evolution upon cycling at 60 °C (100 cycles of C/10 charge and C/2 discharge regime) and (b) capacity evolution vs. cycle number.

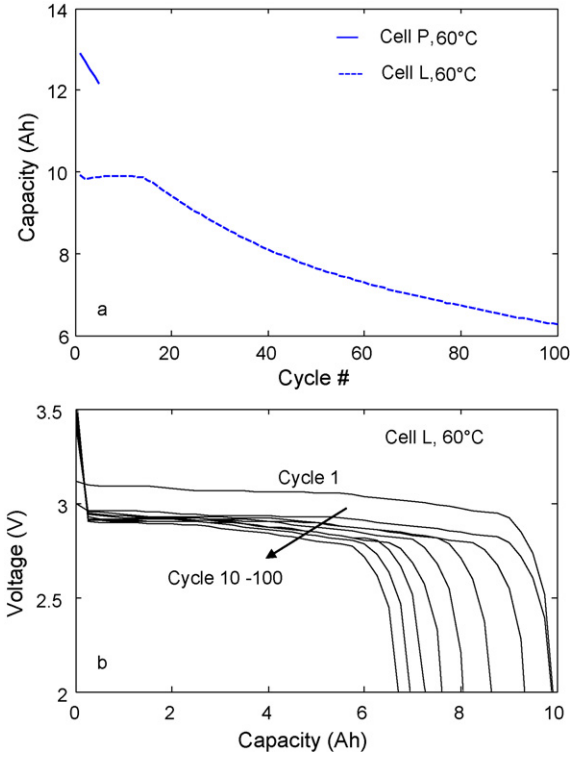

Fig. 3. (a) Capacity loss with cycle number for both cells and (b) evolution of the *V* vs. *Q* curves for Cell L.

12.89 (99%) for the first C/2 cycle. The better C/2 retention in Cell P was due to a modified charge regime, which eliminated the 10 Ah capacity limit in the cutoff condition.

Besides capacity retention, the two cells also exhibited difference in polarization at 60 °C. At low rates such as C/10, the cells did not show much difference in polarization voltage. At high rates such as C/2, the difference in polarization voltage became significant. Cell L showed substantial increase in polarization resistance from the first regime at C/10 to the following two C/2s, as shown in Fig. 2(a), where 200 mV was off in the first C/2 discharge regime and 350 mV in the second. Cell P showed an even more rapid degradation, in which in the first C/2 discharge regime a 500 mV polarization was already observed and remained similar in the second. The polarization resistance was increased by a factor of 4.5 in Cell L and 5 in Cell P from those measured at 25 °C. The same increase was observed in the charge regime as well for both cells.

Fig. 3(a) presents capacity retention with cycle number for Cell L and P. In Cell P, the capacity loss was immediate and the cell lost 4% after 4 cycles. In Cell L, the capacity was stable for about 15 cycles before a quick degradation kicked in. Subsequently, the cell lost 37% of its capacity after 100 cycles. During the life cycle testing, sporadic changes up to ±20% in polarization resistance were observed. Fig. 3(b) displays the progression of the discharge (voltage vs. capacity) curve with cycle number in Cell L at 60 °C. Although the plateau voltage did not show significant changes over cycling, the length of the plateau seems to have changed significantly.

After 100 cycles, Cell L was subjected to 10 extra cycles at C/10 at 60 °C (Fig. 4). Even if the capacity retention seems to fade continuously in the C/2 regimes, it remains stable in the last 10 C/10 regime. The stable retention in the last C/10 cycles suggests that at low rates, the cell can consistently deliver the capacity in accordance with the active material content remained in the cell. Overall, Cell L had lost about 45% of its capacity in the overall life cycle test through the C/2 regimes at 60 °C, according to the capacity determined by the last 10 C/10 cycles.

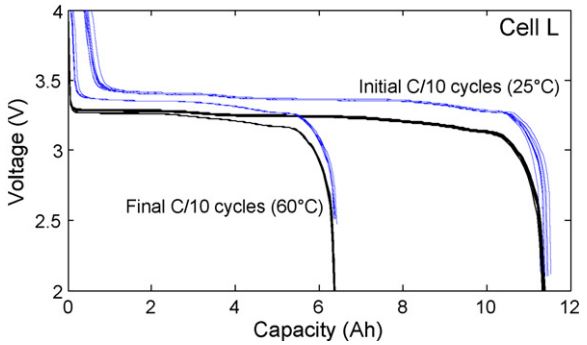

Fig. 4. Initial and final C/10 cycles in the life cycle test of Cell L at 25 °C.

4. Discussion

4.1. Electrochemical behavior and rate capability

As inferred from Fig. 1, the two cells have the same chemistry and present an overall similar electrochemical behavior. From the capacity at C/10 and C/2 it is possible to approximate the Peukert coefficient, which is a representation of rate capability. Cell L presents a slightly better coefficient of 1.012 vs. 1.015 in Cell P; the difference is really slim and the coefficient is in the lower end of the range presented by all commercial LFP cells tested so far. Other cells in each type that underwent different test regimes exhibited similar values, respectively. The incremental capacity signature at C/10 and C/2 (Fig. 5) are consistent with the characteristics of a typical graphite—LFP chemistry [14,16] in which the staging phenomena can be clearly identified. In the negative electrode, the lithium intercalation transforms C to LiC_6 in at least five distinct staging processes (which transform one stage compound to another) [14,16–19]. Each gives a unique IC peak vs. a reference electrode. In the positive electrode, the Li intercalation transforms $FePO_4$ to $LiFePO_4$ reversibly in two non-stoichiometric solid solutions depicting solubility limit in each single phase region and the pseudo-binary Li_xFePO_4–$Li_{1-y}FePO_4$ phase transformation [20,21]. However, the pseudo-binary transformation involves likely more than 95% capacity change in the voltage plateau, which gives a reference potential to the negative electrode reactions. Given the reaction potential and associated capacity in each electrode, the pseudo-binary reaction in the positive electrode, noted as ② ; and the five in the negative electrode,

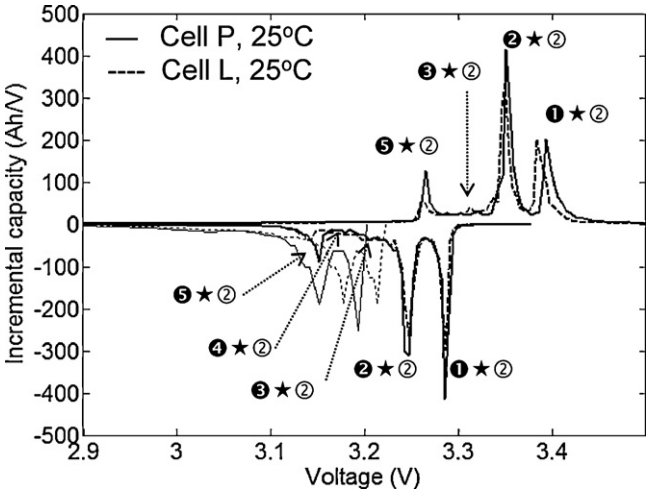

Fig. 5. Incremental capacity curves as signature of the initial state of the two cells (dashed curves are for Cell L and solid curves for Cell P).

❶, ❷, ❸, ❹ and ❺, five IC peaks are identifiable. In our convention, the peak indexed as ❶★② represents reaction ② in the positive electrode convoluting with reaction ❶ in the negative. Comparisons on electrochemical behavior between the two large format cells in Fig. 5 can then be elaborated further as follows:

First, the absence of IC peaks associated with the LFP solid solution regions suggests that the positive electrode active material does not possess any specific features such as nanometer size grains. Secondly, the difference in the peak position between the two cells is inferred most likely by the difference in cell's internal resistance. Our recent study on a batch of 100 $LiCoO_2$ cells showed that variations in the resistance may be substantial [22]. Unfortunately we do not have a sufficient number of cells to provide a statistically meaningful analysis to further elucidate if such differences in the sample cells from both manufacturers are due to different geometries. Nevertheless, in all the cells we tested, the IC peaks associated with Cell L were consistently broader than those associated with Cell P; suggesting that Cell P design results in better electrode kinetics.

It should also be noted that staging 1 in graphite (as denoted by ❶); i.e., the transformation from LiC_{12} to LiC_6; is supposed to account for up to 50% capacity in the negative electrode, whereas staging 2 (❷) is 25%. For a typical LFP cell [12,13], the intensity of peak ❶★② compared to that of ❷★② in the discharge regime is an indicator of the extent of staging 1 in the negative electrode. Since both ❶ and ❷ occur in the same voltage plateau in the positive electrode (②), their intensity and shape should not be influenced by the positive electrode. In Fig. 5, ❶★② is less intense than ❷★②, suggesting that staging 1 only accounts for less than 25% overall capacity. As the peaks display the same shape, the ratio of their intensity will give a good estimate of the extent of staging 1 in each cell. It was 21% for Cell L and 17% for Cell P. Such an underuse of the negative electrode in staging 1 is typical in high power cell design. By providing excess loading with negative electrode, the cell can then exhibit better rate capability, sacrificing specific capacity.

There are other subtle differences in Fig. 5. A peculiar observation is the disparity in the peak separation (i.e., voltage difference) between ❷★② and ❶★② in the charge regime between the two cells. Vice versa, such disparity in the peak separations was also observed in both C/10 and C/2 discharge regimes. The peak separation between the two IC peaks should be constant, since it should be related only to the graphite staging, while the LFP positive electrode remains on a voltage plateau. Reaction ❶★② occurs towards the EOC and there was about 10 mV delay in Cell P (solid line). The origin of such peculiar behavior is not clear from this investigation. However, we can exclude the possibility of contribution from polarization effects because only one peak is affected. We can also exclude the effect from the formation of solid solutions in LFP reaction because the capacity associated with the solid solutions is rather small which should not affect the IC peaks on the negative electrode. We can also exclude the dopant effect. The dopant will change the plateau potential of the positive electrode, thus change the peak positions for all staging reactions, which is not what has been observed. Therefore the 10 mV shift must come from the negative electrode with the stage 2 compound and a delay in the transition from staging 2 to staging 1 process in Cell P. However, the origin of such delay in transition is unknown.

4.2. Temperature effect on the electrochemical behavior

Fig. 6 shows the IC curves associated with C/10 charge and C/10 and C/2 discharge regimes (Fig. 2) at 25 and 60 °C, respectively for

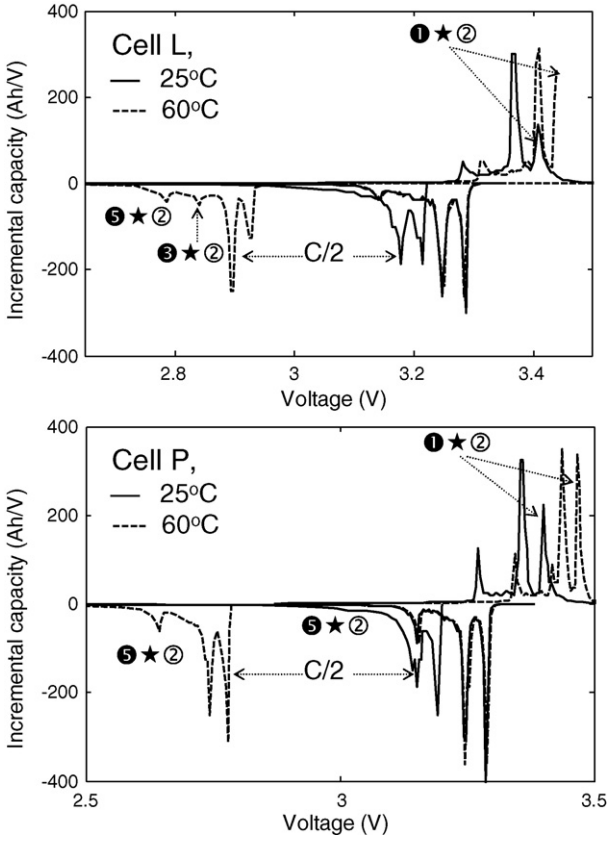

Fig. 6. Comparison of the incremental capacity curves at 25 and 60 °C for both cells.

Cell L and P. As discussed in Section 3, the cell polarization resistance has been increased up to five times when the temperature was raised from 25 to 60 °C. Such an increase is counter-intuitive to what would be expected from the Arrhenius law. A closer look at the IC curves indicates that the kinetics of ❶★② and ❺★② have been improved when the temperature was raised in both cells, as revealed by the more defined features and sharper peaks at 60 °C, which is consistent with an improvement in diffusion and electrode kinetics with temperature in both cases. The fact that in Cell L the polarization resistance did not increase as spontaneously as in Cell P (upon temperature change) may indicate that such resistance increase is not diffusion related, but more likely due to parasitic interfacial phenomena such as the growth of SEI layer [9–12]. The difference in the growth rate of the SEI layer might be related to the different cell geometries; however, after 2 cycles they both appear to experience a similar fivefold increase in resistance.

It should be noted though that the first C/10 cycle in both cell was performed immediately upon a C/10 recharge at 60 °C; therefore, the IC curve was not displaced on the voltage scale from that of 25 °C, as would be expected from the increase of the polarization resistance. Subsequent C/10 charge as shown in Fig. 6 however revealed the displacement in the peak positions between the 25 °C and 60 °C curves, indicating that the effect from the polarization resistance increase has been enacted. This is an indication that the parasitic interfacial process(es) might have taken place in the prior discharge regime. In the subsequent C/2 discharge regime, this "peak displacement" signature has been consistently registered in both cells. It is also important to point out that, in contrast to Cell P, the reaction in ❶★② was not completed in Cell L at 60 °C (due to the charging cutoff at 10 Ah), which led to the low C/2 capacity retention (89%) in Cell L as a result of under-charging.

4.3. Cycling at 60 °C and thermal-induced degradation

From Fig. 3(a) it appears that the two cells did not respond to the temperature rise and thermal degradation in the same way. Cell P lost capacity, although it does not appear as a consequence of rapid (almost spontaneous) increase in polarization resistance, and the capacity fade continues with cycle number. In contrast, Cell L exhibited a rather steady capacity in the first 15 cycles before following suit. Cell L's behavior might be delusive at the outset. The initial steady capacity most likely is an artifact introduced by the charging protocol, which was set to cutoff at 4 V or 10 Ah according to the specifications. In the tests, the cell was discharged at C/10 first, which ended with more than 11 Ah released (see Fig. 2). Subsequently only 10 Ah were recharged, as set by the protocol, leaving with >1 Ah of Li in the positive electrode unused in the cycle at the EOC. Such a constraint in charging protocol resulted in under-charge, and the subsequent C/2 discharge delivered less than 10 Ah as a result of under-charge. The apparent capacity retention in the initial 15 cycles might be the benefit of consuming unused Li in the LFP to compensate capacity fade due to loss of Li inventory or positive electrode active material. When the unused Li in the LFP was exhausted, the cell began to show capacity fade. Fig. 7(a) further reveals the evolution of IC peaks in the charge regime through the 100 C/2 cycles. It clearly shows that in the first 15 cycles the EOC cutoff voltage was not reached, due to the preset capacity cutoff at 10 Ah. Therefore, this protocol induced under-charge has masked the Cell L's initial capacity loss.

Fig. 7(a) reveals additional observations in Cell L at 60 °C. For instance, the fluctuations in the cell voltage as reflected in the peak position for ❷★② and ❺★② indicate the sporadic nature of the polarization resistance which does not follow any particular trend. We do not know the exact cause of such fluctuations but suspect it might be SEI growth related. The shape, intensity and position

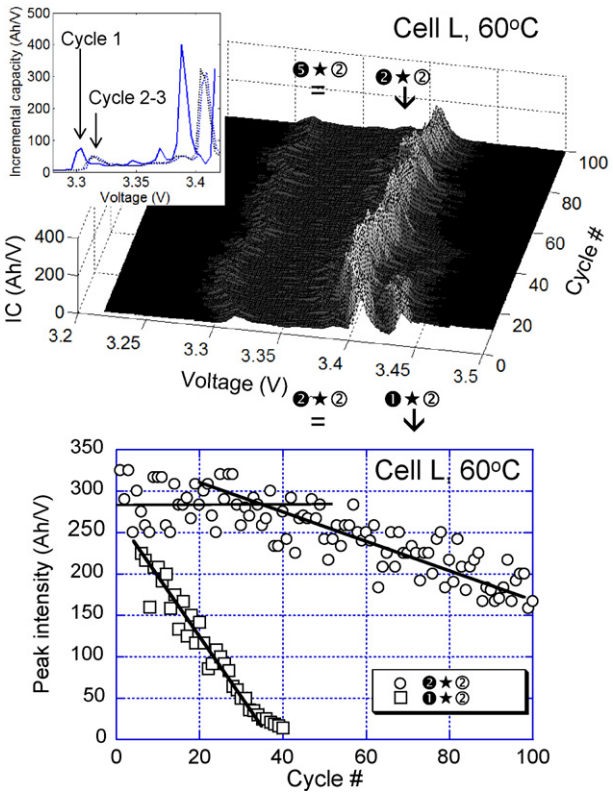

Fig. 7. (a) Evolution of incremental capacity curves with cycle number and (b) evolution of the intensity of peaks ❶★② and ❷★② with cycle number.

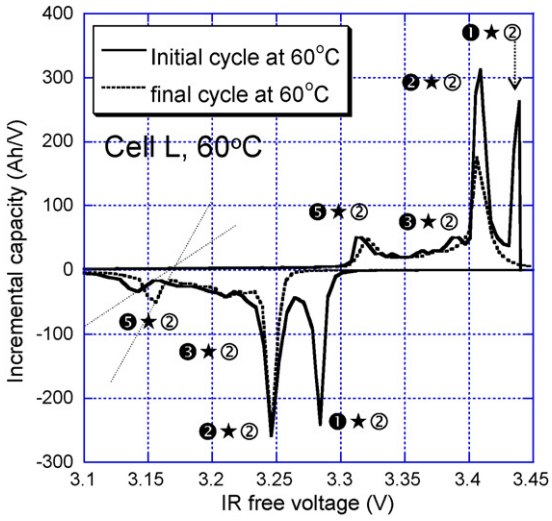

Fig. 8. Incremental capacity curves of initial and final C/10 cycles at 60 °C for Cell L.

of peak ❺★② vary between the first and second cycle noticeably (see inset), but remain relatively stable in the subsequent 98 cycles. Such variation of IC peak shape, intensity and position are associated with the change in polarization resistance. This observation is consistent with those observed in the first two C/2 discharges in Fig. 2, suggesting the coincidence with SEI layer growth, which seems to take 2 cycles to stabilize.

Fig. 7(b) shows the evolution of intensity with peaks ❷★② and ❶★② in Cell L at 60 °C. The intensity of peak ❷★② was scattered but rather constant in average up to the first 40 cycles before decreasing. The intensity of peak ❶★② was decreasing from the outset and disappeared after 40 cycles. It should be noted that, the maximum intensity of peak ❶★② has always been reached before the 10 Ah charge cutoff; therefore, Fig. 7(b) should not be affected by the charging protocol. The disappearance of peak ❶★② coincided with the onset of descending in intensity with peak ❷★②, implying the two could be related. The symptom can be explained by a continuous degradation-induced under-charge. The evolution of C/2 capacity fade shared the same trend with the peak (intensity) evolution, suggesting that under-charge has been an issue.

Fig. 8 presents a comparison of the initial and the final C/10 cycle at 60 °C on a voltage scale that is free of polarization. In the plot, the absence of peak ❶★② in both charge and discharge regime is evident, indicating the disappearing in participation of staging 1 at the end of the life cycle with Cell L at 60 °C.

The fact that the shape and intensity of peak ❺★② in the charge regime remain the same suggests that the reaction kinetics in both electrodes were not altered upon cycling, disregarding the SEI growth. It also indicates that the same amount of negative electrode material is still available after 100 cycles. The disappearance of peak ❶★② and the subsequent decrease in ❷★② intensity indicate that the negative electrode has not been fully utilized anymore at the end of the test. This is consistent with the loss of interaction in staging 1 (❶). We thus conclude that the capacity loss must be attributed to loss of either lithium inventory or positive electrode active material. Unfortunately, without measuring relaxed cell voltage at the EOC and EOD it is not possible to decipher between the two. Andersson and Edström [23], in their study of elevated temperature SEI formation on graphite, suggested that both electrolyte and $LiPF_6$ continue to decompose on the graphite surface through thermal aging or cycling, which could be a possible cause of the loss of Li inventory.

In Fig. 4 it appears that no additional capacity loss was introduced by the 10 C/10 cycles; despite continuous capacity fade was observed in prior C/2 discharge cycles. It is also important to note that the charge regime remains the same in both C/10 and C/2 cycles. This result suggests that the thermal-induced degradation occurs during discharge and is rate-dependent. In Fig. 8, upon analysis of peak ❺★② in the discharge regime, we found that this peak becomes more defined and sharper in shape, higher in intensity, and shifts to a higher voltage, despite the SEI growth, at the end of life cycle. It is indicative that the negative electrode material remains active with Li de-intercalation. The changes in ❺★② peak shape, intensity and position must attribute to kinetic origin. This is supported by the analysis of the onset voltage of the peaks before and after cycling, as shown in Fig. 8. By extrapolating the front slope of the peaks we show that the peaks have the same onset voltage, representing the same electrochemical reaction; in this case, staging 5 (❺). Our earlier interpretation of the IC peak characteristics suggests that peak broadening may often be related to grain size effect in the electrode active material. It is known that graphite upon cycling would result in an amorphous state, which should cause peak broadening. The observed peak thinning after cycling at 60 °C should exclude the contribution from the negative electrode. This behavior should suggest that the grains became smaller upon cycling in the positive electrode. This phenomenon could be attributed to electrochemical milling of grains [24,25] or dissolution of LFP active material [9–12]. Unfortunately, the results that might help to decipher them came from C/2 regime, not C/10; which were also complicated by the noisy resolution of the tester. Deciphering between the two contributions should be deferred to additional experiments in the future.

Electrochemical milling is a mechanical process, known to be quite sporadic due to the nature of cracking arisen from strain–stress field interaction in the solid grains upon Li intercalation. The intra-granular fracture might result in smaller sub-grains completely surrounded by other LFP grains but disconnected from the electron-conductive path provided by the carbon black-binder matrix in the electrode. The inter-granular contact with the electron-conductive path could be disrupted by the intra-granular expansion as well. The loss of electronic contact will impede Li intercalation and render the grains inactive in the electrode reaction. Fracture of grains and loss of contact often take place toward the EOD, as the extent of Li intercalation in LFP grains increases; accompanied with more stress–strain field interactions. At this stage, the grains that were isolated from electron-conductive path may contain high Li content. Such grain isolation will result in loss of active material in the positive electrode subsequently reduce the amount of active Li for intercalation in cycling. In this context, the loss of active material in the positive electrode is the culprit for loss of Li inventory.

The fracture of grains, on the other hand, may produce fresh surface area. If connected with electron-conductive path, the new surface area may actually enhance the kinetics of the electrode reaction. This process may explain the peak thinning observed in Cell L in 60 °C cycle aging. If isolated from electron-conductive path, the new surface may become a reactive site for parasitic reaction to promote SEI layer growth in the presence of electrolyte and Fe(III), when electron transfer cannot be facilitated by the conductive carbon. This mechanism might become another source to induce loss of Li inventory. All the scenarios discussed above may explain the sporadic IC behavior in C/2 discharge regimes observed in Fig. 7. It is known that the un-predictable mechanical behavior could not be replicated consistently in each cycle in a trendy manner; so the electrochemical signatures will bear the same consequence of such behavior.

Dissolution of active material has been proposed to explain the rapid decay of capacity in this chemistry. However, this proposition may face a number of obstacles in explaining all capacity loss phenomena in a consistent manner. For instance, as reported in [13], some experiments showed that change of electrolyte might recover most capacity loss. As stipulated from such observation, it would be difficult to suggest dissolution of grains as a possible explanation of the capacity fade. On the contrary, as the observation stipulates, one can attribute capacity fade to electrolyte wettability issue which is not discernable from the result of electrochemical milling. Indeed, cracked sub-grains might not be accessible by the electrolyte or by electron-conductive path of the carbon black-binder matrix. More controlled experiments are needed to clarify these explanations with more definitive results.

5. Conclusion

In this study we tested and analyzed the behavior of two large format commercial 10 Ah $LiFePO_4$ cells, one prismatic (Cell L) and another cylindrical (Cell P), at 25 and 60 °C. The cells degraded quickly at 60 °C and the degradation was investigated by incremental capacity analysis; an in situ, non-invasive technique; to reveal the possible mechanisms involved. It appears that the degradation is more complicated than those reported in the literature. Two possible origins were identified, namely loss of active material and/or loss of Li inventory, which cannot be distinguished definitively without additional experiments. Electrochemical milling appears to be a possible explanation for the observed degradation as it might cause loss of active material in the positive electrode by isolating grains from the percolation pathway, which may also induce a loss of Li inventory, due to SEI formation on the fresh surface created, especially at elevated temperatures.

References

[1] A.K. Padhi, K.S. Nanjundaswamy, J.B. Goodenough, J. Electrochem. Soc. 144 (1997) 1188.
[2] G. Arnold, J. Garche, R. Hemmer, S. Strobele, C. Vogler, M. Wohlfahrt-Mehrens, J. Power Sources 119 (2003) 247.
[3] J.M. Osorio-Guillen, B. Holm, R. Ahuja, B. Johansson, Solid State Ionics 167 (2004) 221.
[4] S.J. Kwon, C.W. Kim, W.T. Jeong, K.S. Lee, J. Power Sources 137 (2004) 93.
[5] T. Ohzuku, A. Ueda, M. Nagayama, Y. Iwakoshi, H. Komori, Electrochim. Acta 38 (1993) 1159.
[6] H. Arai, S. Okada, H. Ohtsuka, M. Ichimura, J. Yamaki, Solid State Ionics 80 (1995) 261.
[7] W.S. Yoon, K.Y. Chung, K.H. Oh, K.B. Kim, J. Power Sources 119 (2003) 706.
[8] D.C. Li, T. Muta, L.Q. Zhang, M. Yoshio, H. Noguchi, J. Power Sources 132 (2004) 150.
[9] K. Amine, J. Liu, I. Belharouak, Electrochem. Commun. 7 (2005) 669.
[10] H.C. Wu, C.Y. Su, D.T. Shieh, M.H. Yang, N.L. Wu, Electrochem. Solid-State Lett. 9 (12) (2006) A537–A541.
[11] K. Zaghib, N. Ravet, M. Gauthier, F. Gendron, A. Mauger, J.B. Goodenough, C.M. Julien, J. Power Sources 163 (2006) 560–566.
[12] M. Koltypin, D. Aurbach, L. Nazar, B. Ellis, Electrochem. Solid-State Lett. 10 (2) (2007) A40–A44.
[13] M. Maccario, L. Croguennec, F. Le Cras, C. Delmas, J. Power Sources 183 (2008) 411–417.
[14] M. Dubarry, B.Y. Liaw, J. Power Sources 194 (2009) 541.
[15] M. Dubarry, B.Y. Liaw, Electrochim. Acta, submitted.
[16] T. Ohzuku, Y. Iwakoshi, K. Sawai, J. Electrochem. Soc. 140 (1993) 2490.
[17] J. Shim, K.A. Striebel, J. Power Sources 130 (2004) 247.
[18] Y.F. Reynier, R. Yazami, B. Fultz, J. Electrochem. Soc. 151 (2004) A422.
[19] M.E. Spahr, T. Palladino, H. Wilhelm, A. Würsig, D. Goers, H. Buqa, M. Holzapfel, P. Novák, J. Electrochem. Soc. 151 (2004) A1383.
[20] C. Delacourt, P. Poizot, J.-M. Tarascon, C. Masquelier, Nat. Mater. 4 (2005) 254.
[21] C. Delmas, M. Maccario, L. Croguennec, F. Le Gras, F. Weill, Nat. Mater. 7 (2008) 665.
[22] M. Dubarry, N. Vuillaume, B.Y. Liaw, Int. J. Energy Res. 34 (2010) 216–231.
[23] A.M. Andersson, K. Edström, J. Electrochem. Soc. 148 (2001) A1100.
[24] N. Bourgeon, Thèse de doctorat, Nantes, 2003.
[25] J. Morales, R. Trocoli, S. Franger, J. Santos-Pena, Electrochim. Acta 55 (2010) 3075–3082.